2036–2046 *Nucleic Acids Research, 2016, Vol. 44, No. 5* *Published online 15 February 2016*
doi: 10.1093/nar/gkw081

The structure and intermolecular forces of DNA condensates

Jejoong Yoo and Aleksei Aksimentiev*

Center for the Physics of Living Cells, Department of Physics, University of Illinois at Urbana–Champaign, 1110 West Green Street, Urbana, IL 61801, USA

Received October 27, 2015; Revised January 29, 2016; Accepted February 01, 2016

ABSTRACT

Spontaneous assembly of DNA molecules into compact structures is ubiquitous in biological systems. Experiment has shown that polycations can turn electrostatic self-repulsion of DNA into attraction, yet the physical mechanism of DNA condensation has remained elusive. Here, we report the results of atomistic molecular dynamics simulations that elucidated the microscopic structure of dense DNA assemblies and the physics of interactions that makes such assemblies possible. Reproducing the setup of the DNA condensation experiments, we measured the internal pressure of DNA arrays as a function of the DNA–DNA distance, showing a quantitative agreement between the results of our simulations and the experimental data. Analysis of the MD trajectories determined the DNA–DNA force in a DNA condensate to be pairwise, the DNA condensation to be driven by electrostatics of polycations and not hydration, and the concentration of bridging cations, not adsorbed cations, to determine the magnitude and the sign of the DNA–DNA force. Finally, our simulations quantitatively characterized the orientational correlations of DNA in DNA arrays as well as diffusive motion of DNA and cations.

INTRODUCTION

Throughout all kingdoms of life, the DNA of a living organism is found in the form of a compact condensate. In one of the simplest lifeforms—a virus that infects bacteria—DNA can occupy up to 90% of the virus' internal volume (1,2). The high degree of compaction is realized by a molecular motor that uses the energy of ATP hydrolysis to pack DNA into the protein enclosure of a virus, working against an internal pressure that can reach 30 bar (1–4). Genomes of higher organisms, which are stored in much softer compartments, are condensed by polycations. Nucleoid-associated proteins, such as H-NS, fold DNA into the nucleoid structures of prokaryotes whereas nuclear proteins, such as histones and protamines, (3) and biogenic polycations, such as spermidine (Sd^{3+}) and spermine (Sm^{4+}), condense DNA in the nuclei of eukaryotes (5). Mounting evidences suggest that, in addition to efficient storage, cells use DNA condensation as a mechanism for regulation of gene expression (1,6). Other charged macromolecules, such as microtubules or F-actin, can be condensed as well (3,7), suggesting that cells may utilize the condensation phenomenon for various biological functions.

At first glance, DNA condensation is counterintuitive as it suggests attraction between like-charged molecules (8–12). *In vitro* experiments, however, have shown that spontaneous condensation of DNA occurs at room temperature only when polycations of valence +3 or higher are present in the solution (2,3,13–15). Inside the condensates, DNA helices are arranged parallel to one another on a hexagonal lattice; the type and concentration of the polycation determines the characteristic distance between the DNA molecules. Using the osmotic pressure of polymeric osmolytes, Parsegian *et al.* characterized the response of DNA condensates to external mechanical compression (13,15). The measurements of the internal pressure of DNA arrays as a function of the mean inter-DNA distance indicated significant deviations from the predictions of the electrical double layer theory, suggesting that a new physical effect could be at play (13,15).

Despite three decades of scientific inquiry, the phenomenon of DNA condensation remains poorly understood. Based on a mean field approximation, the nonlinear Poisson–Boltzmann (NLPB) theory predicts the interaction of two DNA molecules to be always repulsive, even in the presence of polycations (16). Failure of the NLPB theory to describe DNA condensation was explained by its omission of the highly correlated motion of counterions inside the condensates (17). As discussed in a recent review (10), the correlation effects can be taken into account in both Wigner crystal (16,18–20) and charge-density wave (CDW) models (21–23). The Wigner crystal model prescribed a crystal-like arrangement of cations at the surface of DNA and attractive forces between matching patterns of adsorbed cations. In the CDW models, polycations do not adsorb to DNA but form a density wave between

---

*To whom correspondence should be addressed. Tel: +1 217 333 6495; Fax: +1 866 467 5398; Email: aksiment@illinois.edu the phosphate groups of neighboring DNA helices, driving DNA condensation (10,22,23). Thus, the CDW model is conceptually similar to the 'bridging' model (24–28), where placement of counterions between the DNA duplexes induces effective attraction. In addition to electrostatics of counterions, hydration—structuring of water molecules at the surface of DNA—was proposed to facilitate DNA condensation (14,29). In the absence of experimental methods that could validate or disprove the above models, the mechanism of DNA condensation remained undetermined.

Here, we report the results of explicit-solvent, atomistic molecular dynamics (MD) simulations that characterize the structure, inter-DNA forces and ion atmosphere of DNA condensates in unprecedented detail. In contrast to previous computational studies of inter-DNA forces (28,30–37), our simulations employ a custom parameterization of DNA phosphate–cation interactions (38,39) that have been systematically calibrated against an independent set of experimental data. Our simulations of DNA arrays quantitatively reproduce the experimental pressure–distance relationship for a broad range of ionic conditions, which validates our simulation method. Analysis of the DNA array trajectories and simulations of pairwise DNA–DNA forces reveal the physical origin of the effective attraction between DNA molecules. The results of our MD simulations are used to evaluate competing theories of DNA condensation.

MATERIALS AND METHODS

General MD methods

All MD simulations were carried out using the Gromacs 4.5.5 package (40). See Supplementary Methods Section IIA for the detailed description of the simulation methods. All production simulations employed AMBER99bsc0 force field for DNA (41), TIP3P model of water (42), ion parameters developed by Joung *et al.* (43) subject to custom NBFIX corrections (38) and AMBER-based parameters for spermine ($NH_2(CH_2)_3NH(CH_2)_4NH(CH_2)_3NH_2$) (28) also subject to custom NBFIX corrections (39).

Simulations of DNA arrays

Equilibrated systems containing 64 effectively infinite dsDNA helices ($dG_{20}{\cdot}dC_{20}$) at various NaCl/$MgCl_2$ buffer solutions were obtained following a previously described protocol (38). Briefly, a single DNA duplex was equilibrated in a ~2.5 × 2.5 × 6.8 nm^3 volume of ionic solution; an array of 64 dsDNA helices (~580 000 atoms) was obtained by replicating the pre-equilibrated simulation box. Randomly chosen water molecules were replaced by ions, producing, after several equilibration iterations, the desired concentration of ions outside the DNA array. The final bulk concentrations of Na^+ and Mg^{2+} deviated from their target values by at most 10–20 mM. For Sm^{4+} electrolytes, we found at most 2–3 Sm^{4+} molecules outside the DNA array, which correspond to bulk ion concentration of at most 3 mM.

To build an array of 64 dsDNA molecules at sub-mM $[Sm^{4+}]_b$, a single dsDNA molecule ($dG_{20}{\cdot}dC_{20}$), effectively infinite under the periodic boundary conditions, was simulated for ~30 ns in the presence of 10 Sm^{4+} molecules and explicit water; the simulation system measured ~2.5 × 2.5 × 6.8 nm^3. The equilibrated system was replicated 64 times to position all 64 dsDNA molecules within 11 nm from the origin ($x = 0$, $y = 0$). A pre-equilibrated volume of water was added to make a system that measures ~29 × 29 × 6.8 nm^3. A small number of water molecules was randomly replaced with Na^+ and Cl^- ions to bring the concentration of NaCl to 200 mM before equilibration. The resulting system was equilibrated for ~50 ns before the production run. During the equilibration, the half-harmonic restraining potential (see the next paragraph) kept DNA inside the cylindrical volume of 11-nm radius.

All simulations of the DNA array systems were carried out in the presence of a half-harmonic potential that applied restraining forces to DNA phosphorus atoms to confine the DNA molecules within the prescribed cylindrical volume. The half-harmonic potential was defined as $V^{\text{wall}}(r) = 0.5k(r - R)^2$ for $r > R$ and 0 otherwise, where r was the distance from the phosphorus atom to the center of the DNA array, R was the radius of the confining cylinder, and k was the force constant (100 kJ/mol nm^2); the restraining potential did not apply to water or ions. In the production runs, DNA concentration was controlled by changing R. In such a setup, the internal pressure in the DNA array equals to the pressure exerted by the half-harmonic potential on the DNA. Error bars of the pressure were estimated using standard deviations of 10-ns block averages. The setup of our simulations mimic the experimental situation where osmolytes, such as long chains of PEG polymer, are used to apply pressure to a DNA array (13).

Simulations of pairwise PMF

The systems used for the calculations of the potential of mean force (PMF) between a pair of dsDNA molecules were prepared by placing two 20-bp fragments of dsDNA ($dG_{20}{\cdot}dC_{20}$) in a hexagonal prism volume of water, which was ~13 nm on a side within the $x - y$ plane and 6.8 nm along the z axis. The DNA molecules were parallel to the z axis and covalently bound to themselves across the periodic boundary of the system. The size of the simulation system was chosen to minimize the finite size effects even when the separation between the DNA molecules was 4–5 nm (44). Specific ionic conditions were obtained by replacing randomly chosen water molecules with ions. In the case of spermine solutions, the initial system was built by duplicating the pre-equilibrated DNA-spermine complex. Each system was equilibrated for at least 10 ns at a specific ionic condition. Umbrella sampling simulations were performed on the equilibrated systems. The force constant of the harmonic umbrella potentials was 1000 kJ/mol nm^2. The reaction coordinate was defined as the distance between the centers of mass of the DNA molecules projected onto the xy plane, ξ; the range of ξ in the umbrella sampling was from 23 to 40 Å with 1 Å spacing. For each window, we performed 10 ns of equilibration and ~50 ns of production runs. In our umbrella sampling simulations, the DNA molecules were free to rotate and slide with respect to each other. The weighted histogram analysis method (WHAM) was used for the reconstruction PMF from the umbrella sampling simulations (45).

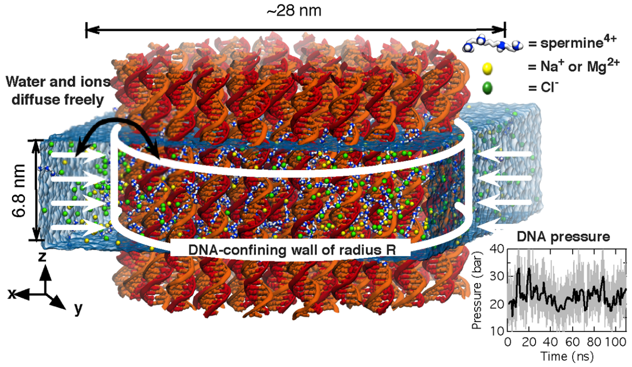

Figure 1. Setup of DNA array simulations. An array of 64 dsDNA molecules (red and orange) submerged in a rectangular volume of electrolyte solution (semitransparent surface) is subject to a half-harmonic well potential (white cylinder). Each DNA duplex contains 20 bp in the simulation cell. Each strand of the duplex is covalently linked to itself across the periodic boundary of the system, making the DNA molecule effectively infinite. Only the phosphorous atoms of DNA are subject to the half-harmonic potential, allowing water and ions to pass in and out of the DNA bundle. The force applied by the half-harmonic potential to DNA reports on the internal pressure in the DNA array. (Inset) A representative trace of the internal pressure in a DNA array during an MD simulation. In this particular simulation, the bulk concentration of sodium, $[Na^+]_b$, was 250 mM; the radius of the confining well potential $R = 12$ nm.

A protocol used to evaluate the contributions of individual interaction types to the pairwise PMFs (46–48) is described in Supplementary Methods Section IIB.

RESULTS AND DISCUSSION

MD simulations of DNA arrays

In biological systems, DNA condensation occurs by either mechanical compression or with the help of condensing agents such as polyamines. Here, we model biological DNA condensates using an array of 64 parallel DNA molecules confined to a semipermeable cylinder, Figure 1. The confining potential applied only to atoms of DNA, allowing water and ions to freely exchange between the volume of the DNA condensate and the buffer solution. In equilibrium, the average force exerted by the confining potential on DNA reports on the average internal pressure in the DNA array. Typically, a ∼100-ns MD trajectory was sufficient to determine the internal pressure; the inset in Figure 1 shows the fluctuations of the pressure during a representative MD run. Repeating the simulation of the DNA array at several values of the confining cylinder radius *R*, we obtained the dependence of the DNA pressure on the mean inter-axial distance between nearest neighbor DNA helices, which hereafter we refer to as the inter-DNA distance.

According to Parsegian *et al.* (13,29,49), mechanical compression of DNA using a semi-permeable membrane is ‘thermodynamically equivalent’ to DNA condensation produced by the osmotic stress of dissolved polymers, which is the method used to experimentally characterize DNA condensates. Thus, the setup of our MD simulations permits direct comparison with experiment.

The simulated structural and mechanical properties of DNA arrays quantitatively matched the experimental observations (13,15). In agreement with the X-ray diffraction measurements (13,15), DNA molecules were found to arrange on a hexagonal lattice, Figure 2A(i), B(i) and C(i); the valence of the buffer cations influenced the mean inter-DNA distance. The simulated dependence of the DNA array pressure on the inter-DNA distance quantitatively matched the experimentally measured dependences (13,15) in the case of the pure monovalent (Na$^+$) buffer solution, Figure 2A(iii), as well as for the mixture of divalent (Mg^{2+}), Figure 2B(iii), or tetravalent (Sm^{4+}), Figure 2B(iii), ions with Na$^+$. A slight overestimation of the DNA array pressure at 20 mM bulk concentration of Mg^{2+} ($[Mg^{2+}]_b = 20$ mM), Figure 2B(iii), is likely caused by Na$^+$ ions that were present at 200 mM concentration in the bulk region of the MD system (outside the confining potential) but absent in the corresponding experimental measurement (13).

Taking into account the size and complexity of our simulation systems, conformational sampling and reproducibility can be an issue, in particular for the system containing tetravalent cations, Sm^{4+}. To demonstrate adequate sampling and reproducibility of our DNA array simulations, we performed a replicate simulation of the DNA array system starting from the following extreme initial conditions: all Sm^{4+} molecules were placed outside the DNA array. The results of the replicate simulation, Supplementary Figure S1 and Figure 2C(iii), are in quantitative agreement with the results of our original simulations, indicating their convergence. SM Section I provides a detailed discussion of sampling and convergence issues.

Ion atmosphere

Our simulations of the DNA arrays elucidated a correlation between the local configuration of the DNA molecules and the distribution of cations within the DNA condensates (50). In the case of a monovalent buffer solution ($[Na^+]_b = 250$ mM), Na$^+$ ions are distributed over the entire internal volume of the condensate accumulating locally between two DNA molecules, Figure 2A(i). For a mixture of divalent and monovalent cations ($[Mg^{2+}]_b = 20$ mM and $[Na^+]_b = 200$ mM), the charge of cations (mainly of Mg^{2+} ions, Supplementary Figure S2A and B) was observed to localize more preferentially between DNA molecules that formed closer than average contacts, Figure 2B(i). The accumulation of Mg^{2+} between proximal DNA pairs as well as the direct readout of the DNA pressure, *cf.* Figure 2A(iii) and B(iii), indicate that Mg^{2+} reduces DNA pressure more efficiently than Na$^+$ does. At sub-mM $[Sm^{4+}]_b$, which is a simulation condition where the total charge of Sm^{4+} cations exactly compensates the total charge of DNA, spontaneous condensation of DNA was observed in both simulation and experiment, despite the presence of Na$^+$ ions at 200 mM concentration in the buffer solution (35–37). The charge of Sm^{4+} cations was observed to localize at the interface of condensed DNA pairs, Figure 2C(i) and Supplementary Figure S2C and D, which, as we show later, indicates the presence of bridging cations (24–28). Consistent with the previous computational study (35,51), Sm^{4+} cations were observed to adsorb to the major grooves of DNA helices, Figure 2C(i). Figure 3A illustrates a representative configuration of Sm^{4+} cations around a DNA duplex. At the cen-

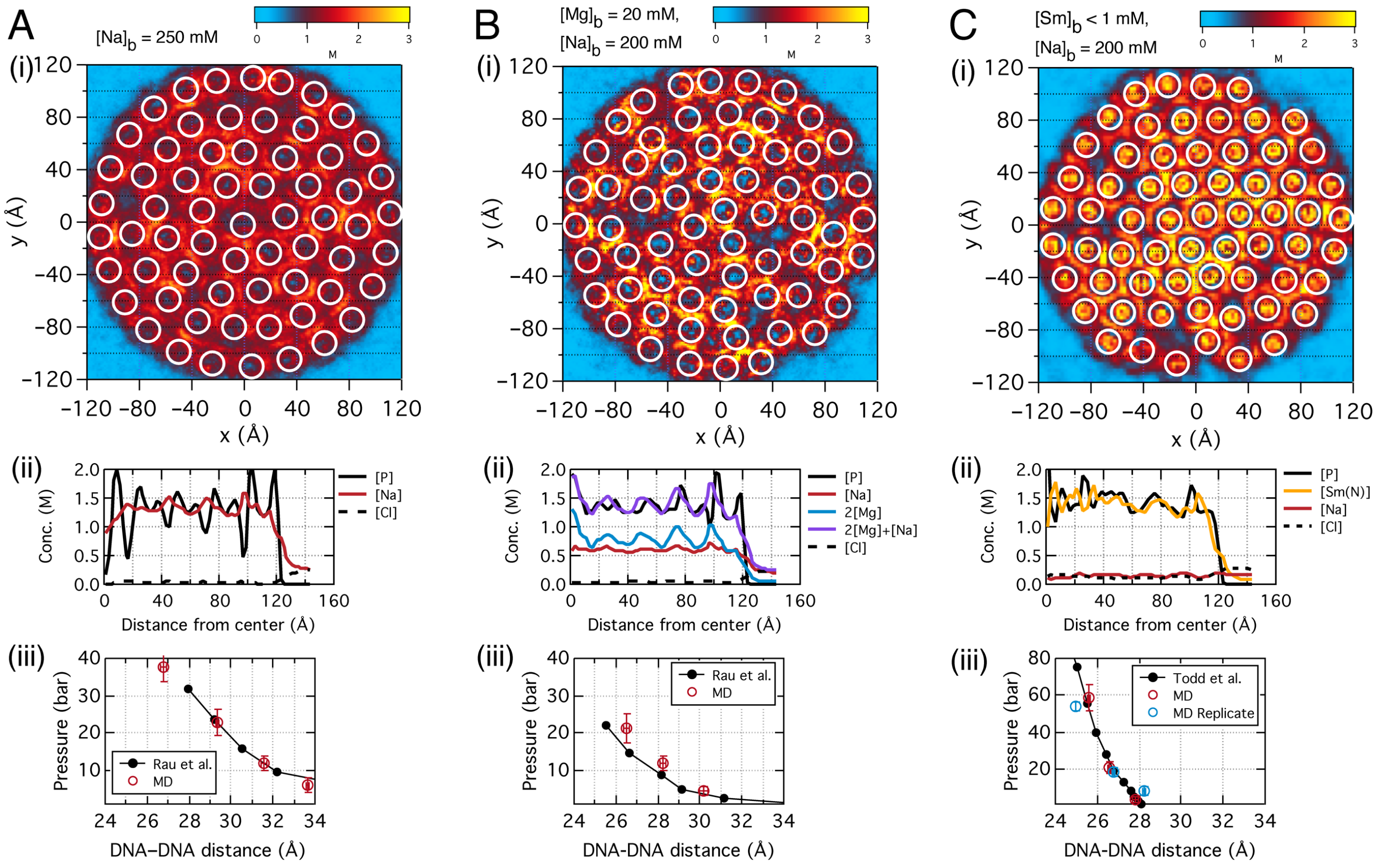

Figure 2. MD simulations of DNA arrays. (**A**) Internal structure,radial ion distribution and the internal pressure versus inter-DNA distance for DNA array systems at $[\mathrm{Na}^+]_\mathrm{b} = 250$ mM. (i) Local distribution of cation charge (heat map) and the arrangement of the DNA helices (white circles) in the cross section of a DNA array at $R = 12$ nm. The diameter of each white circle is 2 nm. The data were averaged over the last 20 ns fragment of a ∼100 ns trajectory and over the *z* axis. (ii) The local concentration of charged species versus the distance from the center of the DNA array. The number density of each species was determined using 2 Å cylindrical shells and the last 20 ns segment of the production run. (iii) The simulated internal pressure of a DNA array versus the nearest-neighbor DNA–DNA separation (red circles). Each data points represents an average of the entire MD trajectory (>100 ns) at fixed *R*; the mean inter-DNA distance was changed by setting *R* to 11, 12, 13 and 14 nm. The black line shows the corresponding experimental dependence (13,15). (**B**, **C**) Same as in panel A but at the following bulk electrolyte conditions: $[\mathrm{Mg}^{2+}]_\mathrm{b} = 20$ mM and $[\mathrm{Na}^+]_\mathrm{b} = 200$ mM (B) and sub-mM $[\mathrm{Sm}^{4+}]_\mathrm{b}$ and $[\mathrm{Na}^+]_\mathrm{b} = 200$ mM (C). The local cation charge concentration was computed as $2[\mathrm{Mg}^{2+}]+[\mathrm{Na}^+]$ (B) and $4[\mathrm{Sm}^{4+}]+[\mathrm{Na}^+]$ (C). Experimental data in panel C correspond to $[\mathrm{Sm}^{4+}]_\mathrm{b} = 2$ mM (15).

ter of the condensate, Figure 2C(i), bridging Sm^{4+} cations force DNA to arrange on a compact hexagonal lattice. At the boundary of the condensate, the arrangement is less compact, reflecting the lack of bridging cations at the outer boundary of the array.

The distributions of ions observed in our simulations characterize the competition of Mg^{2+} or Sm^{4+} ions with Na^+ ions for neutralization of the DNA charge in the DNA condensate. For the 20-mM $[\mathrm{Mg}^{2+}]_\mathrm{b}$ / 200-mM $[\mathrm{Na}^+]_\mathrm{b}$ mixture, the concentration of Mg^{2+} charge inside the DNA array is almost the same as the concentration of Na^+ charge, Figure 2B(ii), indicating a stronger affinity of Mg^{2+} to DNA than that of Na^+ (36,37). The local cation charge, $2[\mathrm{Mg}^{2+}]+[\mathrm{Na}^+]$, almost exactly matches the local concentration of the DNA phosphate groups, Figure 2B(ii). For the sub-mM $[\mathrm{Sm}^{4+}]_\mathrm{b}$ / 200-mM $[\mathrm{Na}^+]_\mathrm{b}$ mixture, the DNA charge is neutralized almost completely by Sm^{4+} ions, Figure 2C(ii); the concentration of either Na^+ and Cl^- inside the array is similar to its buffer value. In qualitative agreement with the counterion condensation theory that assumes deposition of counterions at the ideal surface of DNA (52), we find cations carrying a higher charge to localize more strongly near the surface of DNA. The quantitative deviation of the theory (8,53) from experiment (13,14) may be explained by our observation that Sm^{4+} is not fully deposited to the surface of a single DNA but localized in the space between the surfaces of the neighboring DNA helices.

DNA–DNA forces in a DNA condensate are pairwise

Given that the surface-to-surface distance between DNA molecules in a DNA array is only 2 to 7 Å and that the concentration of mobile charges exceeds 1 M, one could expect DNA condensation to exhibit features of a cooperative phenomenon due to water structuring (8). One specific theoretical prediction was the breakdown of pairwise additivity of inter-DNA forces in dense DNA arrays under low salt conditions (54,55). As pointed out by Bloomfield (8), the presence of cooperativity (or breakdown of pairwise additivity) can be an indicator of the significant contribution of water structuring to DNA condensation. To evaluate the

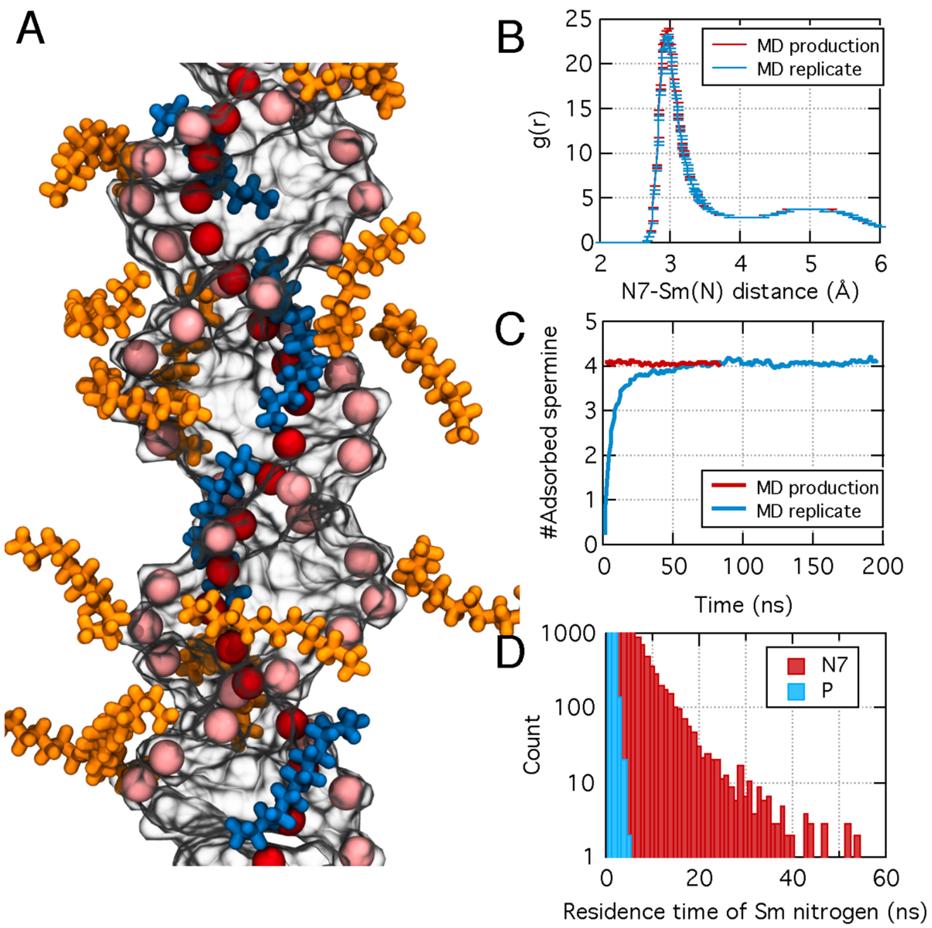

Figure 3. Adsorption of Sm^{4+} to DNA. (**A**) A representative conformation of Sm^{4+} molecules near a 20-bp dsDNA molecule (gray semitransparent surface). Four Sm^{4+} molecules adsorbed to DNA are shown in blue whereas 10 Sm^{4+} molecules loosely associated with DNA are shown in orange. The N7 nitrogen and phosphorus (P) atoms of DNA are shown as red and pink spheres, respectively. (**B**) The radial distribution functions, $g(r)$, of Sm^{4+} nitrogen atoms with respect to the N7 atoms of DNA computed from the replicate (blue) and production (red) simulations. (**C**) The number of Sm^{4+} molecules adsorbed at a 20-bp dsDNA duplex as a function of the simulation time for the replicate (blue) and production (red) simulations. (**D**) Residence time of Sm^{4+} nitrogen atoms within the direct contact distance of N7 (red) and P (blue) atoms. The contact distance was determined as the first peak of $g(r)$: 4 and 4.5 Å for N7 and P atoms, respectively. Data in panels B and D were obtained by analyzing the last 80 ns of the respective MD trajectories of the $R = 12$ nm DNA array systems.

degree of cooperativity in the simulated DNA condensates, we computed the pairwise PMF $\Delta G(\xi)$ between two parallel DNA molecules and the average pairwise inter-DNA force $f(\xi)$ as a function of the inter-DNA distance ξ; Figure 4A illustrates the simulation setup. In qualitative agreement with the results of our DNA array simulations and experiment (13), pairwise DNA–DNA forces were always repulsive ($f(\xi) > 0$) in monovalent (Na^+) and divalent (Mg^{2+}) electrolytes regardless of the concentration, Figure 4B and C. Furthermore, the pairwise force in the presence of Sm^{4+} was attractive ($f(\xi) < 0$) within the 28 to 40 Å range of the inter-DNA distance even at sub-mM $[Sm^{4+}]_b$ (Figure 4D). In broad agreement with the thermodynamic measurement that revealed a rather small free energy change per basepair in polycation-induced condensation (0.01–0.1 k_BT per basepair) (8), the computed free energy change associated with the reduction of inter-DNA distance from 40 to 28 Å was only $\sim 0.1\ k_BT$ per basepair (Figure 4D).

Assuming that the pairwise inter-DNA forces between nearest neighbors in a DNA array determine the internal pressure of the array, the mean inter-DNA force $\bar{f}$ can be determined from the mean pressure $\bar{\pi}$ as $\bar{f} = \bar{\pi}\bar{\xi}/\sqrt{3}$, where $\bar{\xi}$ is the mean inter-DNA distance (13). Using the above expression, we plot the average pairwise inter-DNA force computed from the simulated internal pressure of the DNA arrays (open black circles) alongside the pairwise force observed in our simulation of two DNA molecules (solid lines), bottom row of Figure 4B–D. Comparison of the inter-DNA force extracted from the PMF simulations to the mean inter-DNA force observed in the DNA array simulations shows that inter-DNA forces in DNA condensates are pairwise for all electrolyte conditions studied (Figure 4B–D). One can arrive at the same conclusion by comparing the experimental estimates of the pairwise force (13,15) (solid triangles) with the results of the pairwise force simulation (Figure 4B–D).

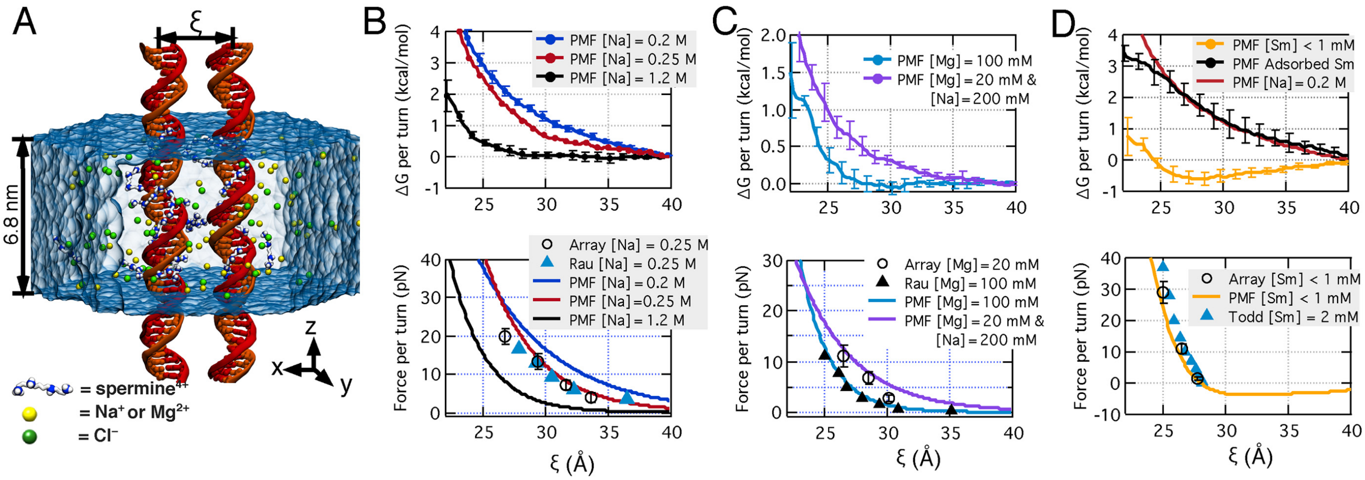

Figure 4. Pairwise inter-DNA forces. (**A**) Setup for the calculation of a pairwise potential of mean force (PMF) between two DNA molecules. A pair of parallel 20 bp fragments of dsDNA is submerged in a hexagonal prism volume of electrolyte solution (semitransparent surface); the DNA molecules are effectively infinite under the periodic boundary conditions. (**B**–**D**) Pairwise PMF (top) and the effective DNA–DNA force (bottom) as a function of the inter-DNA distance for electrolytes containing exclusively Na^+ ions (B), a mixture of Mg^{2+} and Na^+ ions (C), and a mixture of Sm^{4+} and Na^+ ions (D). The background concentration of Na^+ in the systems containing Mg^{2+} and Sm^{4+} is 200 mM. A copy of the ΔG dependence at $[Na^+] = 200$ mM (panel B) is shown in panel D to simplify comparison of the ΔG curves. The pairwise forces were computed by taking derivatives of the double-exponential fit to the respective ΔG curves. Black circles in the bottom plots indicate the average DNA–DNA force computed from the DNA array simulations.

DNA attraction is produced by non-contact bridging cations

Having established the pairwise nature of DNA–DNA forces in a DNA condensate, we determined the role of adsorbed Sm^{4+} molecules in DNA condensation. In the Wigner crystal models (16,18), 'correlation holes' formed by the adsorbed counterions induce DNA condensation (10). In our simulations of the DNA array systems, each 20-basepair DNA fragment reproducibly had four Sm^{4+} molecules adsorbed to its surface (Figure 3A–C), which amount to only a 40% charge neutralization, considerably less than 90% assumed by the Wigner crystal models. Because of the strong attractions between Sm^{4+} amine groups and N7 atoms of guanine, amine groups of adsorbed Sm^{4+} reside in contact with N7 atoms significantly longer than 5 ns. In contrast, the residence time of the amine groups near DNA phosphates is at most 5 ns, Figure 3D.

To determine if adsorption of Sm^{4+} to DNA can produce an attractive interaction between two DNA molecules, we repeated the inter-DNA PMF calculations for a system of two 20-basepair DNA molecules each having four Sm^{4+} cations adsorbed to the major groove and surrounded by 200 mM $[Na^+]_b$. At all DNA–DNA separations, Sm^{4+} cations remained bound to the major grooves of the respective DNA molecules for the entire duration (60 ns per window) of the simulations. Comparison of the PMFs computed in the presence and absence of adsorbed Sm^{4+} molecules and 200 mM $[Na^+]_b$, Figure 4D, clearly shows that having Sm^{4+} adsorbed at the surface of DNA does not make the inter-DNA interaction less repulsive. Thus, the effective DNA–DNA attraction observed in our simulations of the Sm^{4+} systems cannot be accounted for by the Wigner crystal models (16,18).

Analysis of cation distributions identified the concentration of bridging cations as a determinant of the magnitude and direction of the inter-DNA force, consistent with the predictions of the CDW (22,23) or ion bridging (24–28) models. For a system of two DNA molecules submerged in 200 mM $[Na^+]_b$ electrolyte, Figure 5A plots the average cation density within the plane normal to the DNA molecules at inter-DNA distance $\xi = 30$ Å. Figure 5B and C shows the average cation densities observed after addition of 20 mM $[Mg^{2+}]_b$ or sub-mM $[Sm^{4+}]_b$ to the 200 mM $[Na^+]_b$ system. Supplementary Figures S3, S4 and S5 show the cation distributions for the entire range of inter-DNA distances. In all three systems, cations are seen to both adsorb to the grooves of DNA, which is indicated by local maxima of concentration inside white circles representing DNA molecules, and loosely bind to the DNA's phosphate groups, which is indicated by a halo outside the white circles. Unlike Na^+ and Mg^{2+}, Sm^{4+} concentration is significantly enriched when two ionic halos overlap, consistent with the distributions observed in our DNA array simulations.

For quantitative comparison of the cation distributions, the bottom panels of Figure 5A–C shows one-dimensional concentration profiles obtained by averaging the two-dimensional distributions. The overlap of the Sm^{4+} halos increases the concentration of Sm^{4+} by 3-fold (Figure 5C); no significant enrichment is observed for Na^+ and Mg^{2+} ions (Figure 5A and B). The abundance of interstitial Sm^{4+} cations is correlated with the observation of the attractive inter-DNA forces, which gives support to the CDW (22,23) and ion bridging (24,26,28,56,57) models of DNA condensation. In contrast to the results of the previous MD study (28), we find that direct bridging of the two DNA molecules by the same spermine cations is not required for DNA condensation. For inter-DNA distances less than 30 Å, less than one Sm^{4+} cation formed, on average, a simultaneous contact with two DNA molecules (Supplementary Figure S6); no such contacts were observed for larger inter-DNA distances characterized by attractive DNA–DNA forces.

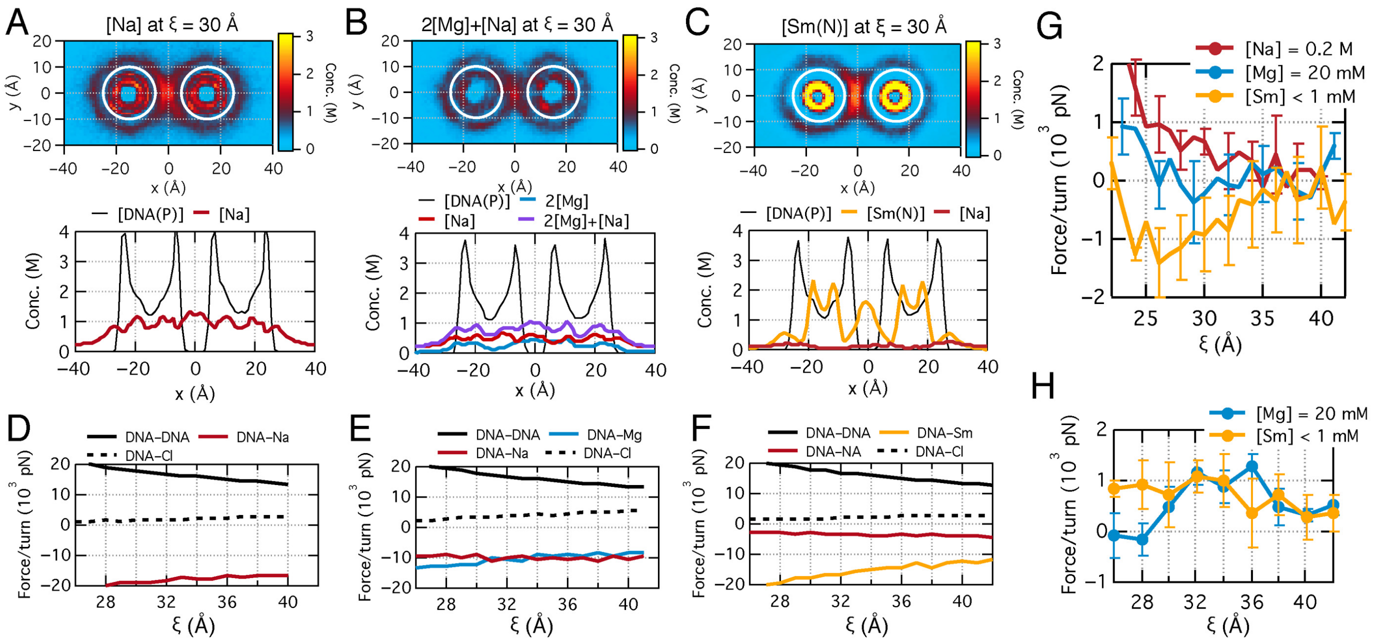

Figure 5. Analysis of pairwise inter-DNA forces. (**A–C**) (Top) Local charge concentration of cations around a pair of dsDNA molecules at $[\mathrm{Na}^+]_\mathrm{b} = 200$ mM (panel A), $[\mathrm{Mg}^{2+}]_\mathrm{b} = 20$ mM and $[\mathrm{Na}^+]_\mathrm{b} = 200$ mM (panel B) and sub-mM $[\mathrm{Sm}^{4+}]_\mathrm{b}$ and $[\mathrm{Na}^+]_\mathrm{b} = 200$ mM (panel C). To simplify comparison with the concentration of the DNA's phosphate groups, the charge concentration is plotted in molar unit (1 M = ∼0.6 e nm^{-3}). The heat maps were obtained by averaging over the z axis (the directions of the DNA molecules) and the corresponding simulation trajectory. White circles indicate the locations of the DNA helices. (Bottom) The concentration of DNA phosphorous atoms (black), Mg^{2+}, Na^+ and Sm^{4+} ions along the x axis computed by averaging over the z axis, the corresponding simulation trajectory and the $y = [-10, 10]$ Å region of the corresponding system. (**D–F**) Contribution of individual molecular species to the Coulomb component of the effective DNA–DNA force at $[\mathrm{Na}^+]_\mathrm{b} = 200$ mM (panel D), $[\mathrm{Mg}^{2+}]_\mathrm{b} = 20$ mM and $[\mathrm{Na}^+]_\mathrm{b} = 200$ mM (panel E), and sub-mM $[\mathrm{Sm}^{4+}]_\mathrm{b}$ and $[\mathrm{Na}^+]_\mathrm{b} = 200$ mM (panel F). (**G**) The contribution of all but water molecular species to the Coulomb component of the effective DNA–DNA forces at $[\mathrm{Na}^+]_\mathrm{b} = 200$ mM, $[\mathrm{Mg}^{2+}]_\mathrm{b} = 20$ mM and $[\mathrm{Na}^+]_\mathrm{b} = 200$ mM, and sub-mM $[\mathrm{Sm}^{4+}]_\mathrm{b}$ and $[\mathrm{Na}^+]_\mathrm{b} = 200$ mM. (**H**) The contribution of water to the effective DNA–DNA force at $[\mathrm{Mg}^{2+}]_\mathrm{b} = 20$ mM and $[\mathrm{Na}^+]_\mathrm{b} = 200$ mM, and at sub-mM $[\mathrm{Sm}^{4+}]_\mathrm{b}$ and $[\mathrm{Na}^+]_\mathrm{b} = 200$ mM.

The results of our calibration osmotic pressure simulations suggest that the standard MD force fields considerably overestimate the strength of amine–phosphate interactions (39), which may have contributed to the observation of the direct bringing mechanism in the previous simulation study (28). For example, at inter-DNA separation of 25 Å, ref. (28) reports an attractive force of ∼80 pN per DNA turn whereas the force is experimentally measured to be repulsive, 36 pN in magnitude (15). In contrast, the average effective force observed in our simulations at the same conditions is repulsive, about ∼30 pN per DNA turn. Furthermore, the most likely distance between two DNA molecules in a Sm^{4+} solution observed in our simulations (28 Å) is consistent with the experimental value (also 28 Å) (15), whereas a much smaller value, ∼23 Å, was reported from the simulation where direct bridging was observed (28). The quantitative agreement between our simulation results and experiment suggests that the non-contact bridging mechanism observed in our work is more plausible than the direct bridging mechanism suggested previously (28).

Electrostatics, not hydration, produces DNA condensation

To quantitatively characterize the role of cations in determining the DNA–DNA force, we computed the electrostatic contribution to the pairwise inter-DNA force from individual ionic species and DNA phosphates (20,58,59). The direct DNA–DNA electrostatic force (black lines in Fig-

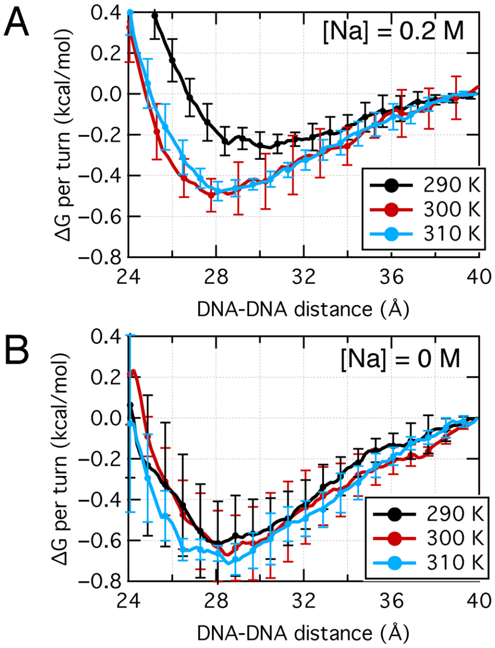

Figure 6. Temperature dependence of inter-DNA interactions. (**A** and **B**) Comparison of the pairwise PMFs obtained from the simulations of two effectively infinite DNA molecules in the presence of sub-mM $[\mathrm{Sm}^{4+}]_\mathrm{b}$ at 290, 300, 310 K at $[\mathrm{Na}^+]_\mathrm{b} = 200$ mM (panel A) and $[\mathrm{Na}^+]_\mathrm{b} = 0$ mM (panel B). Apart from temperature and ion concentration, all other simulation conditions were identical to those depicted in Figure 4.

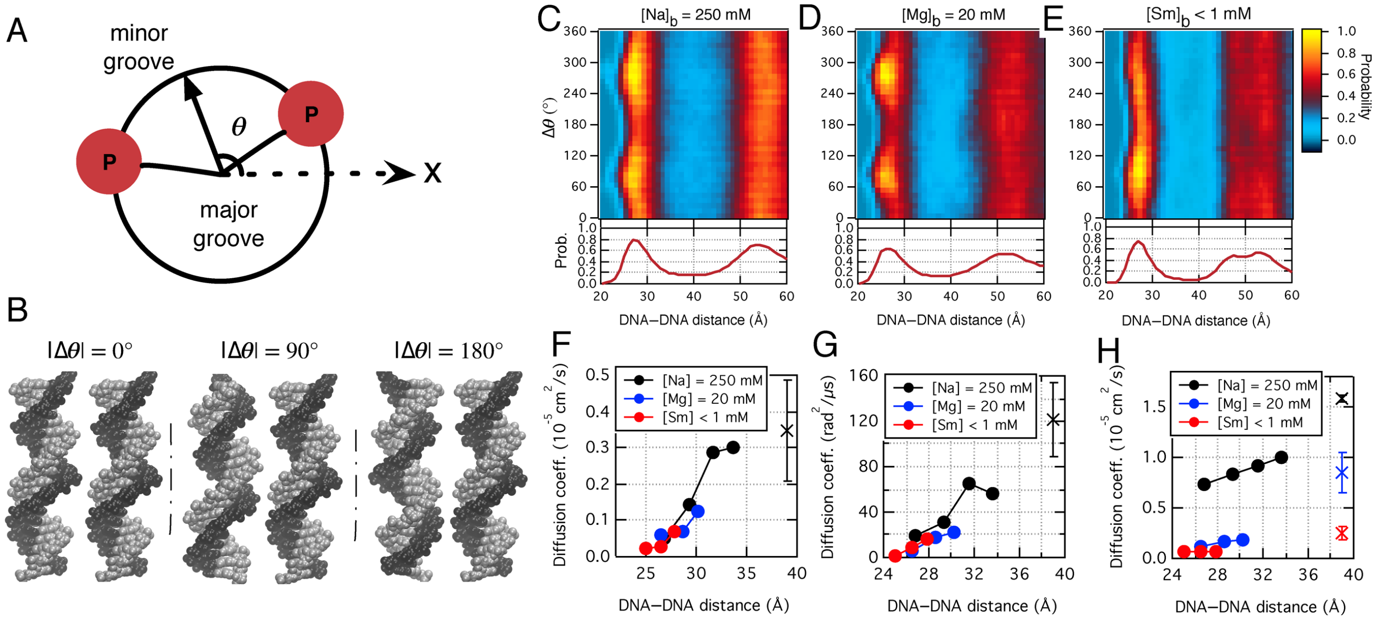

Figure 7. Azimuthal correlation and self-diffusion in DNA arrays. (**A**) Schematic of a DNA cross-section. Each red circle (denoted 'P') indicates the intersection of the DNA backbone with the cross-section plane. The two arcs connecting the red circles illustrate the minor and major grooves of the DNA helix. The azimuthal orientation of a DNA helix is defined as the angle (θ) that a vector connecting the center of the DNA helix and the center of the minor groove arc forms with the x axis. (**B**) Representative conformation of two DNA helices oriented at a mutual azimuthal angle $\Delta\theta$ of 0° (left), 90° (center) and 180° (right). (**C**–**E**) The mutual orientation ($\Delta\theta$) and the CoM separation of two DNA helices in DNA array simulations ($R = 12$ nm) shown as probability heat maps. The ionic conditions featured in these panels are: $[\mathrm{Na}^+]_\mathrm{b} = 250$ mM (panel C), $[\mathrm{Mg}^{2+}]_\mathrm{b} = 20$ mM and $[\mathrm{Na}^+]_\mathrm{b} = 200$ mM (panel D), and sub-mM $[\mathrm{Sm}^{4+}]_\mathrm{b}$ and $[\mathrm{Na}^+]_\mathrm{b} = 200$ mM (panel E). (**F**–**H**) Self-diffusion in DNA condensates. Diffusion coefficients characterizing the stochastic displacement of DNA in the direction of the helix (panel F), the stochastic rotation of DNA (panel G), and the 3D diffusive motion of cations (panel H) as a function of the mean nearest neighbor DNA–DNA distance. Each panel features data sets obtained at three different ion buffer conditions. The 'x' mark indicates the average and the standard deviation of the values observed in the two-DNA systems at $\xi = 37$, 38, 39 and 40 Å.

ure 5D–F) is about three orders of magnitude larger than the electrolyte-mediated inter-DNA force (Figure 4B–D) and monotonically decreases with the inter-DNA distance. The repulsive direct DNA–DNA force is almost completely compensated by the attractive force from cations (Figure 5D). For the 20 mM $[\mathrm{Mg}^{2+}]_\mathrm{b}$ / 200 mM $[\mathrm{Na}^+]_\mathrm{b}$ mixture, the contribution from Mg^{2+} is of the same order as that from Na^+, Figure 5E; the contribution from Sm^{4+} ions dominates over that from Na^+ despite the sub-mM concentration of Sm^{4+} (Figure 5C). The force between DNA and Cl^- is always repulsive and considerably smaller than the force from cations; its magnitude increases with the inter-DNA distance, indicating depletion of Cl^- when DNA helices are in proximity. The net electrostatic force contributed by all ionic species (including DNA) is attractive (negative) only in the presence of Sm^{4+} (Figure 5G) which indicates the electrostatic nature of the forces driving DNA condensation. A decomposition of the cation–DNA forces according to the location of the cations identified bridging cations as the cause of the attractive electrostatic force (Supplementary Figure S7).

Our force decomposition calculations suggest that water contributes to mutual repulsion of DNA, not to the DNA attraction. To illustrate this point, we calculated the contribution to the inter-DNA force from all water molecules taking into account both van der Waals and electrostatic components (Figure 5H). The force contributed by water is always repulsive (>0) and does not considerably depend on the cation type. Note that, through sampling over many local water configurations realized by the MD trajectory, our force decomposition analysis does include the entropic contribution associated with the conformational degrees of freedom of the solvent. Although direct comparison of our results with the predictions of the hydration force theory (14,14,29) is not possible, our results indicate that water does not play a major direct role in inducing inter-DNA attraction.

Comparison with thermodynamic data

Thermodynamics data suggest that DNA condensation induced by multivalent cations is driven by changes in entropy whereas changes in enthalpy oppose the condensation (49,60,61). Increasing temperature and, hence, the system's entropy is found to make DNA condensation more favorable (60), however, whether that change of entropy is caused by release of water (entropy from hydration) (49) or by release of counterions (entropy from electrostatics) (60) has remained undetermined. To identify the entropy increase mechanism, we repeated our calculations of the pairwise DNA–DNA PMF at neutralizing Sm^{4+} concentration (20 Sm^{4+} molecules per system) at 290, 300 or 310 K for $[\mathrm{Na}^+]_\mathrm{b} = 0$ or 200 mM (Figure 6).

At $[\mathrm{Na}^+]_\mathrm{b} = 200$ mM, the inter-DNA free energy was significantly less favorable for DNA–DNA attraction at 290 K compared to that at higher temperatures (Figure 6A). This result is consistent with experimental thermodynamic data for mixed solutions of Na^+ and polycations (60). However, at $[Na^+]_b = 0$ mM, our simulations determined no significant temperature dependence of the inter-DNA PMF (Figure 6B). Thus, our simulations indicate that the temperature dependence of the DNA–DNA PMF originates from the release of cations (in the $[Na^+]_b = 200$ mM system), supporting the argument expressed in ref. (60). This conclusion is consistent with the results of our force decomposition analysis described in the previous section.

Orientational correlations in DNA condensates

It has been suggested that the helical structure of a DNA molecule can induce correlations in the mutual orientation of neighboring DNA molecules forming a DNA condensate (19,62,63). Analysis of our DNA array simulations confirms this prediction (Figure 7A–E). Using the minor groove of a DNA helix as an indicator of the DNA orientation, (Figure 7A and B) we characterized the probability of observing a pair of DNA molecules forming a prescribed relative azimuthal angle $\Delta\theta$ at a prescribed inter-DNA distance (Figure 7C–E). Consistent with the theoretical prediction (19) and X-ray scattering data (62,63), the mutual orientation of the nearest neighbor DNA helices is more probable at $|\Delta\theta| \approx 90^\circ$. The azimuthal correlation becomes stronger as DNA arrays become more compressed, regardless of the cation type (Supplementary Figure S8). In all systems studied, the azimuthal correlation disappears beyond the nearest neighbor DNA molecules.

Diffusion and friction

Recent experiments have shown that ions can significantly affect packaging and ejection of DNA to and from viral shells (64–68). Berndsen *et al.* observed dramatic slow down of DNA dynamics inside the virus (65). Grayson *et al.* measured DNA ejection at 10 mM Na^+ to be 5–10 times faster than at 10 mM Mg^{2+} (64). Keller *et al.* reported heterogeneous non-equilibrium dynamics of DNA packaging and ejection caused by the presence of spermidine cations (67). Experiments, however, could not determine whether the effects were caused by the changes in the DNA–DNA friction, internal pressure of the virus or ion-specific interactions (66).

Analysis of our DNA array simulations suggests the microscopic cause of the experimental observations. Figure 7F and G displays the diffusion coefficients for longitudinal translation and rotation, respectively, of DNA helices in the DNA arrays versus the average inter-DNA distance for several ionic conditions. Both diffusion coefficients decrease with the inter-DNA distance and do not explicitly depend on the type or concentration of ions. The diffusivity of cations within the DNA condensates is approximately a quarter of the corresponding bulk value (Figure 7H). At both 10 mM Na^+ and 10 mM Mg^{2+}, the inter-DNA distance inside a viral capsid is ∼30 Å (2). According to our simulations, the inter-DNA friction (inverse of the DNA diffusivity) is similar at the two ionic conditions and hence the 10-fold slowdown of DNA ejection at 10 mM Mg^{2+} (64) should be caused by a lower internal pressure of the capsid. In contrast, spontaneous condensation of DNA by Sm^{4+} in a partially filled viral capsid will reduce the translational and rotational diffusion of DNA by 5-fold (Figure 7F and G), which may introduce a heterogeneity into the DNA packaging process (67).

CONCLUSIONS

In summary, we have used all-atom MD simulations to elucidate the physical mechanism of ion-mediated DNA condensation. The results of our simulations support the ion-bridging model, whereby DNA attraction is produced by cations localized between the DNA helices. Our study demonstrates the ability of all-atom MD simulations to provide quantitative, accurate information about dense DNA systems, opening exciting opportunities for future work in the area of synthetic DNA nanostructures (69), the phase behavior of DNA liquid crystal (70) and DNA packaging in viral capsids and cell nuclei (2,71).

SUPPLEMENTARY DATA

Supplementary Data are available at NAR online.

ACKNOWLEDGEMENTS

This work was supported by the National Science Foundation grant PHY-1430124. The authors acknowledge supercomputer time at the Blue Waters Sustained Petascale Facility (University of Illinois) and at the Texas Advanced Computing Center (Stampede, allocation award MCA05S028).

FUNDING

National Science Foundation [PHY-1430124]. Funding for open access charge: NSF [PHY-1430124].

Conflict of interest statement. None declared.

REFERENCES

1. Knobler,C.M. and Gelbart,W.M. (2009) Physical chemistry of DNA viruses. *Annu. Rev. Phys. Chem.*, **60**, 367–383.
2. Qiu,X., Rau,D.C., Parsegian,V.A., Fang,L.T., Knobler,C.M. and Gelbart,W.M. (2011) Salt-dependent DNA-DNA spacings in intact bacteriophage λ reflect relative importance of DNA self-repulsion and bending energies. *Phys. Rev. Lett.*, **106**, 028102.
3. Wong,G. C.L. and Pollack,L. (2010) Electrostatics of strongly charged biological polymers: ion-mediated interactions and self-organization in nucleic acids and proteins. *Annu. Rev. Phys. Chem.*, **61**, 171–189.
4. Smith,D.E., Tans,S.J., Smith,S.B., Grimes,S., Anderson,D.L. and Bustamante,C. (2001) The bacteriophage phi29 portal motor can package DNA against a large internal force. *Nature*, **413**, 748–752.
5. Eisenberg,T., Knauer,H., Schauer,A., Büttner,S., Ruckenstuhl,C., Carmona-Gutierrez,D., Ring,J., Schroeder,S., Magnes,C., Antonacci,L. *et al.* (2009) Induction of autophagy by spermidine promotes longevity. *Nat. Cell. Biol.*, **11**, 1305–1314.
6. Dekker,J., Marti-Renom,M.A. and Mirny,L.A. (2013) Exploring the three-dimensional organization of genomes: Interpreting chromatin interaction data. *Nat. Rev. Genet.*, **14**, 390–403.
7. Sanders,L.K., Xian,W., Guáqueta,C., Strohman,M.J., Vrasich,C.R., Luijten,E. and Wong,G.C.L. (2007) Control of electrostatic interactions between F-actin and genetically modified lysozyme in aqueous media. *Proc. Natl. Acad. Sci. U.S.A.*, **104**, 15994–15999.
8. Bloomfield,V.A. (1997) DNA condensation by multivalent cations. *Biopolymers*, **44**, 269–282.
9. Grosberg,A.Y., Nguyen,T.T. and Shklovskii,B.I. (2002) Colloquium: the physics of charge inversion in chemical and biological systems. *Rev. Mod. Phys.*, **74**, 329–345.

10. Kornyshev,A., Lee,D., Leikin,S. and Wynveen,A. (2007) Structure and interactions of biological helices. *Rev. Mod. Phys.*, **79**, 943–996.
11. Bloomfield,V.A. (1996) DNA condensation. *Curr. Opin. Struct. Biol.*, **6**, 334–341.
12. Kornyshev,A.A. (2010) Physics of DNA: unravelling hidden abilities encoded in the structure of 'the most important molecule'. *Phys. Chem. Chem. Phys.*, **12**, 12352–12378.
13. Rau,D.C., Lee,B. and Parsegian,V.A. (1984) Measurement of the repulsive force between polyelectrolyte molecules in ionic solution: hydration forces between parallel DNA double helices. *Proc. Natl. Acad. Sci. U.S.A.*, **81**, 2621–2625.
14. Rau,D.C. and Parsegian,V.A. (1992) Direct measurement of the intermolecular forces between counterion-condensed DNA double helices. Evidence for long range attractive hydration forces. *Biophys. J.*, **61**, 246–259.
15. Todd,B.A., Parsegian,V.A., Shirahata,A., Thomas,T.J. and Rau,D.C. (2008) Attractive forces between cation condensed DNA double helices. *Biophys. J.*, **94**, 4775–4782.
16. Shklovskii,B.I. (1999) Wigner crystal model of counterion induced bundle formation of rodlike polyelectrolytes. *Phys. Rev. Lett.*, **82**, 3268–3271.
17. Qiu,X., Giannini,J., Howell,S.C., Xia,Q., Ke,F. and Andresen,K. (2013) Ion competition in condensed DNA arrays in the attractive regime. *Biophys. J.*, **105**, 984–992.
18. Rouzina,I. and Bloomfield,V.A. (1996) Macroion attraction due to electrostatic correlation between screening counterions. 1. Mobile surface-adsorbed ions and diffuse ion cloud. *J. Phys. Chem.*, **100**, 9977–9989.
19. Kornyshev,A.A. and Leikin,L. (1997) Theory of interaction between helical molecules. *J. Chem. Phys.*, **107**, 3656–3674.
20. Kornyshev,A.A. and Leikin,S. (1999) Electrostatic Zipper Motif for DNA Aggregation. *Phys. Rev. Lett.*, **82**, 4138–4141.
21. Oosawa,F. (1968) Interaction between parallel rodlike macroions. *Biopolymers*, **6**, 1633–1647.
22. Deserno,M., Arnold,A. and Holm,C. (2003) Attraction and ionic correlations between charged stiff polyelectrolytes. *Macromolecules*, **36**, 249–259.
23. Angelini,T.E., Liang,H., Wriggers,W. and Wong,G. C.L. (2003) Like-charge attraction between polyelectrolytes induced by counterion charge density waves. *Proc. Natl. Acad. Sci. U.S.A.*, **100**, 8634–8637.
24. Raspaud,E., Chaperon,I., Leforestier,A. and Livolant,F. (1999) Spermine-induced aggregation of DNA, nucleosome, and chromatin. *Biophys. J.*, **77**, 1547–1555.
25. Schellman,J.A. and Parthasarathy,N. (1984) X-ray diffraction studies on cation-collapsed DNA. *J. Mol. Biol.*, **175**, 313–329.
26. Raspaud,E., de la Cruz,M.O., Sikorav,J.L. and Livolant,F. (1998) Precipitation of DNA by polyamines: a polyelectrolyte behavior. *Biophys. J.*, **74**, 381–393.
27. Dai,L., Mu,Y., Nordenskiöld,L., Lapp,A. and van der Maarel,J. R.C. (2007) Charge structure and counterion distribution in hexagonal DNA liquid crystal. *Biophys. J.*, **92**, 947–958.
28. Dai,L., Mu,Y., Nordenskiöld,L. and van der Maarel,J. R.C. (2008) Molecular dynamics simulation of multivalent-ion mediated attraction between DNA molecules. *Phys. Rev. Lett.*, **100**, 118301.
29. Leikin,S., Parsegian,V.A., Rau,D.C. and Rand,R.P. (1993) Hydration forces. *Annu. Rev. Phys. Chem.*, **44**, 369–395.
30. Savelyev,A. and Papoian,G.A. (2007) Inter-DNA electrostatics from explicit solvent molecular dynamics simulations. *J. Am. Chem. Soc.*, **129**, 6060–6061.
31. Luan,B. and Aksimentiev,A. (2008) DNA attraction in monovalent and divalent electrolytes. *J. Am. Chem. Soc.*, **130**, 15754–15755.
32. Guldbrand,L., Nilsson,L.G. and Nordenskiöld,L. (1986) A Monte Carlo simulation study of electrostatic forces between hexagonally packed DNA double helices. *J. Chem. Phys.*, **85**, 6686–6698.
33. Lyubartsev,A.P. and Nordenskiöld,L. (1995) Monte Carlo simulation study of ion distribution and osmotic pressure in hexagonally oriented DNA. *J. Phys. Chem.*, **99**, 10373–10382.
34. Lyubartsev,A.P. and Nordenskiöld,L. (1997) Monte Carlo simulation study of DNA polyelectrolyte properties in the presence of multivalent polyamine ions. *J. Phys. Chem. B*, **101**, 4335–4342.
35. Korolev,N., Lyubartsev,A.P., Nordenskiöld,L. and Laaksonen,A. (2001) Spermine: an 'invisible' component in the crystals of B-DNA. A grand canonical Monte Carlo and molecular dynamics simulation study. *J. Mol. Biol.*, **308**, 907–917.
36. Korolev,N., Lyubartsev,A.P., Rupprecht,A. and Nordenskiöld,L. (1999) Competitive binding of Mg2+, Ca2+, Na+, and K+ ions to DNA in oriented DNA fibers: experimental and Monte Carlo simulation results. *Biophys. J.*, **77**, 2736–2749.
37. Korolev,N., Lyubartsev,A.P., Rupprecht,A. and Nordenskiöld,L. (2001) Competitive substitution of hexammine cobalt(III) for Na+ and K+ ions in oriented DNA fibers. *Biopolymers*, **58**, 268–278.
38. Yoo,J. and Aksimentiev,A. (2012) Improved parametrization of Li^+, Na^+, K^+, and Mg^{2+} ions for all-atom molecular dynamics simulations of nucleic acid systems. *J. Phys. Chem. Lett.*, **3**, 45–50.
39. Yoo,J. and Aksimentiev,A. (2016) Improved parameterization of amine–carboxylate and amine–phosphate interactions for molecular dynamics simulations using the CHARMM and AMBER force fields. *J. Chem. Theory Comput.*, **12**, 430–443.
40. Hess,B., Kutzner,C., van der Spoel,D. and Lindahl,E. (2008) GROMACS 4: algorithms for highly efficient, load-balanced, and scalable molecular simulation. *J. Chem. Theory Comput.*, **4**, 435–447.
41. Perez,A., Marchan,I., Svozil,D., Sponer,J., Cheatham,T.E., Laughton,C.A. and Orozco,M. (2007) Refinement of the AMBER force field for nucleic acids: improving the description of α/γ conformers. *Biophys. J.*, **92**, 3817–3829.
42. Jorgensen,W.L., Chandrasekhar,J., Madura,J.D., Impey,R.W. and Klein,M.L. (1983) Comparison of simple potential functions for simulating liquid water. *J. Chem. Phys.*, **79**, 926–935.
43. Joung,I.S. and Cheatham,T.E. (2008) Determination of alkali and halide monovalent ion parameters for use in explicitly solvated biomolecular simulations. *J. Phys. Chem. B*, **112**, 9020–9041.
44. Yoo,J. and Aksimentiev,A. (2012) Competitive binding of cations to duplex DNA revealed through molecular dynamics simulations. *J. Phys. Chem. B*, **116**, 12946–12954.
45. Kumar,S., Rosenberg,J.M., Bouzida,D., Swendsen,R.H. and Kollman,P.A. (1992) The weighted histogram analysis method for free-energy calculations on biomolecules. I. The method. *J. Comput. Chem.*, **13**, 1011–1021.
46. Darve,E. and Pohorille,A. (2001) Calculating free energies using average force. *J. Chem. Phys.*, **115**, 9169–9183.
47. Hénin,J. and Chipot,C. (2004) Overcoming free energy barriers using unconstrained molecular dynamics simulations. *J. Chem. Phys.*, **121**, 2904–2914.
48. Yoo,J. and Cui,Q. (2013) Membrane-mediated protein-protein interactions and connection to elastic models: a coarse-grained simulation analysis of gramicidin A association. *Biophys. J.*, **104**, 128–138.
49. Leikin,S., Rau,D.C. and Parsegian,V.A. (1991) Measured entropy and enthalpy of hydration as a function of distance between DNA double helices. *Phys. Rev. A*, **44**, 5272–5278.
50. Lipfert,J., Doniach,S., Das,R. and Herschlag,D. (2014) Understanding nucleic acid-ion interactions. *Annu. Rev. Biochem*, **83**, 813–841.
51. Luan,B. and Aksimentiev,A. (2010) Electric and electrophoretic inversion of the DNA charge in multivalent electrolytes. *Soft Matter*, **6**, 243–246.
52. Manning,G.S. (1969) Limiting laws and counterion condensation in polyelectrolyte solutions I. Colligative properties. *J. Chem. Phys.*, **51**, 924–933.
53. Wilson,R.W. and Bloomfield,V.A. (1979) Counterion-induced condensation of deoxyribonucleic acid. A light-scattering study. *Biochemistry*, **18**, 2192–2196.
54. Podgornik,R. and Parsegian,V.A. (1998) Charge-fluctuation forces between rodlike polyelectrolytes: pairwise summability reexamined. *Phys. Rev. Lett.*, **80**, 1560–1563.
55. Ha,B.-Y. and Liu,A.J. (1998) Effect of non-pairwise-additive interactions on bundles of rodlike polyelectrolytes. *Phys. Rev. Lett.*, **81**, 1011–1014.
56. de la Cruz,M.O., Belloni,L., Delsanti,M., Dalbiez,J.P., Spalla,O. and Drifford,M. (1995) Precipitation of highly charged polyelectrolyte solutions in the presence of multivalent salts. *J. Chem. Phys.*, **103**, 5781–5791.
57. Tolokh,I.S., Pabit,S.A., Katz,A.M., Chen,Y., Drozdetski,A., Baker,N., Pollack,L. and Onufriev,A.V. (2014) Why double-stranded RNA resists condensation. *Nucl. Acids Res.*, **42**, 10823–10831.

58. Ma,L., Yethiraj,A., Chen,X. and Cui,Q. (2009) A computational framework for mechanical response of macromolecules: application to the salt concentration dependence of DNA bendability. *Biophys. J.*, **96**, 3543–3554.
59. Fenley,M.O., Manning,G.S. and Olson,W.K. (1992) Electrostatic persistence length of a smoothly bending polyion computed by numerical counterion condensation theory. *J. Phys. Chem.*, **96**, 3963–3969.
60. Matulis,D., Rouzina,I. and Bloomfield,V.A. (2000) Thermodynamics of DNA binding and condensation: isothermal titration calorimetry and electrostatic mechanism.. *J. Mol. Biol.*, **296**, 1053–1063.
61. Korolev,N., Berezhnoy,N.V., Eom,K.D., Tam,J.P. and Nordenskiöld,L. (2009) A universal description for the experimental behavior of salt-(in)dependent oligocation-induced DNA condensation.. *Nucl. Acids Res.*, **37**, 7137–7150.
62. Strey,H.H., Wang,J., Podgornik,R., Rupprecht,A., Yu,L., Parsegian,V.A. and Sirota,E.B. (2000) Refusing to twist: demonstration of a line hexatic phase in DNA liquid crystals. *Phys. Rev. Lett.*, **84**, 3105–3108.
63. Leforestier,A. and Livolant,F. (2009) Structure of toroidal DNA collapsed inside the phage capsid. *Proc. Natl. Acad. Sci. U.S.A.*, **106**, 9157–9162.
64. Grayson,P., Han,L., Winther,T. and Phillips,R. (2007) Real-time observations of single bacteriophage λ DNA ejections in vitro. *Proc. Natl. Acad. Sci. U.S.A.*, **104**, 14652–14657.
65. Berndsen,Z.T., Keller,N., Grimes,S., Jardine,P.J. and Smith,D.E. (2014) Nonequilibrium dynamics and ultraslow relaxation of confined DNA during viral packaging. *Proc. Natl. Acad. Sci. U.S.A.*, **111**, 8345–8350.
66. Liu,T., Sae-Ueng,U., Li,D., Lander,G.C., Zuo,X., Jönsson,B., Rau,D., Shefer,I. and Evilevitch,A. (2014) Solid-to-fluid-like DNA transition in viruses facilitates infection. *Proc. Natl. Acad. Sci. U.S.A.*, **111**, 14675–14680.
67. Keller,N., delToro,D., Grimes,S., Jardine,P.J. and Smith,D.E. (2014) Repulsive DNA-DNA interactions accelerate viral DNA packaging in phage Phi29. *Phys. Rev. Lett.*, **112**, 248101.
68. Migliori,A.D., Keller,N., Alam,T.I., Mahalingam,M., Rao,V.B., Arya,G. and Smith,D.E. (2014) Evidence for an electrostatic mechanism of force generation by the bacteriophage T4 DNA packaging motor. *Nat. Commun.*, **5**, 4173.
69. Seeman,N.C. (2010) Nanomaterials based on DNA. *Annu. Rev. Biochem*, **79**, 65–87.
70. Nakata,M., Zanchetta,G., Chapman,B.D., Jones,C.D., Cross,J.O., Pindak,R., Bellini,T. and Clark,N.A. (2007) End-to-end stacking and liquid crystal condensation of 6 to 20 base pair DNA duplexes. *Science*, **318**, 1276–1279.
71. DeRouchey,J., Hoover,B. and Rau,D.C. (2013) A comparison of DNA compaction by arginine and lysine peptides: a physical basis for arginine rich protamines. *Biochemistry*, **52**, 3000–3009.